BOLETIN DE LA SOCIEDAD ESPAÑOLA DE
Cerámica y Vidrio
www.elsevier.es/bsecv

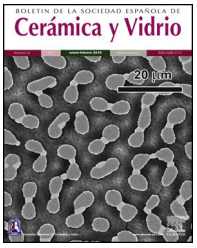

Characterization and bioactivity behavior of sol–gel derived bioactive vitroceramic from non-conventional precursors

*Lindsey Alejandra Quintero Sierra**, *Diana Marcela Escobar*

Biomaterials Research Group, Engineering Faculty, University of Antioquia, Colombia

ARTICLE INFO

Article history:
Received 19 April 2018
Accepted 9 July 2018
Available online 27 July 2018

Keywords:
Vitroceramic
Bioactivity
Non-conventional precursors
Hydroxyapatite layer

ABSTRACT

The use of biomaterials has proven to be an excellent alternative in tissue regeneration due to the many possibilities they can offer. Bioactive glasses are a group of bioceramics that are being used in bone tissue engineering thanks to their biological properties, one of those being the bioactivity behavior. These bioactive glasses require a stabilization process by thermal treatments that partially crystallize the structure acquiring a vitroceramic state. In this study, sol–gel-derived bioactive vitroceramic was synthesized in a ternary system using non-conventional calcium and phosphate precursors in order to evaluate its bioactivity in the presence of simulated body fluid (SBF). The obtained bioactive vitroceramic was evaluated through XRD, FTIR, Raman and SEM to measure its chemical composition and morphology. The bioactivity test was carried out using cylindrical discs made with bioactive vitroceramic; those discs were analyzed in 7 and 14 days of exposition. The formed layer was studied with XRD, FTIR, SEM and EDX analysis. The results have shown that synthesized bioactive vitroceramic has similar composition and crystallinity of those reported in the same system indicating the appropriate use of different precursors. Likewise, the bioactivity behavior showed the formation of a non-crystalline hydroxyapatite layer on bioactive vitroceramic surface with a Ca/P ratio similar to that in bone, which means that the synthesized material can be used in bone tissue engineering.

Caracterización y comportamiento bioactivo de vitrocerámica bioactiva sintetizada por vía sol-gel usando precursores no convencionales

Palabras clave:
Vitrocerámica
Bioactividad
Precursores no convencionales
Capa de hidroxiapatita

RESUMEN

El uso de los biomateriales ha probado ser una excelente alternativa en la regeneración de tejidos debido a las múltiples posibilidades que pueden ofrecer. Los vidrios bioactivos son un grupo de biocerámicos que se han usado en la Ingeniería de Tejido Óseo gracias a sus propiedades biológicas, una de ellas el comportamiento bioactivo. Estos vidrios bioactivos requieren un tratamiento térmico para estabilizar la estructura adquiriendo un estado

* *Corresponding author.*
E-mail address: lindsey.alejandra@gmail.com (L.A. Quintero Sierra).
https://doi.org/10.1016/j.bsecv.2018.07.003

vitrocerámico. En este trabajo se sintetizó una vitrocerámica bioactiva por el método de sol-gel en un sistema ternario usando precursores no convencionales como fuentes de calcio y fósforo con el fin de evaluar su comportamiento bioactivo en presencia de fluido corporal simulado. La vitrocerámica bioactiva obtenida se evaluó por XRD, FTIR, espectroscopía Raman y SEM para medir su composición química y morfología. El ensayo de bioactividad se realizó usando discos fabricados con la vitrocerámica bioactiva sintetizada; estos discos se sumergieron en SBF por 7 y 14 días. La capa formada en su superficie se analizó por medio de XRD, FTIR, SEM y EDX. Los resultados mostraron que la vitrocerámica sintetizada presenta una composición y cristalinidad similar a aquellos reportados en el mismo sistema lo que indica que los precursores usados son apropiados para este tipo de síntesis. Igualmente, el comportamiento bioactivo demostró que se depositó una capa de hidroxiapatita no cristalina en la superficie del material con una relación Ca/P similar a la del hueso, esto indica que la vitrocerámica bioactiva sintetizada tiene potencial para ser usado en la Ingeniería de Tejido Óseo.

Introduction

Throughout tissue regeneration strategies, the use of biomaterials is an interesting alternative due to their biological and mechanical properties. These properties along with the possibility for structural and compositional manipulations allow the improvement of biocompatibility in the final product. One of the biomaterials with those properties is the bioactive glasses. They are a group of ceramic materials worldwide used as bone filling and reinforcement in tissue engineering. These materials can stimulate osteogenesis by inducing a biological response at the biomaterial–bone interface that promotes the proliferation and differentiation of human osteoblasts [1,2]. Furthermore, these kinds of materials have in their structures different elements such as silicon, phosphorous, sodium, calcium, among others. Most of bioactive glasses synthesized so far employ the silicon-based composition previously reported by Hench et al. [3,4]. According to Hench, differences in silicon concentrations reduces or promotes tissue bonding with both hard and soft tissues; he also indicated that lower proportions of silicon promotes bonding with soft tissues, whereas higher proportions reduce any kind of bonding [3].

The first bioactive glass (Bioglass 45S5) was discovered by Larry Hench et al. in 1971 [4], since then a variety of glass compositions were studied. Nevertheless, different results found in the literature [5–7] show that not just composition but also the preparation method influence on the final structure and the resultant biological properties of the material. The sol–gel synthesis has been widely used as an appropriate method to obtain bioactive glasses with small and different morphologies, such as powders, coatings, fibers or 3D porous scaffolds both micro and nanosized [8,9]. Lower crystallinity, uses less processing temperature than melt-quenching process [10] and the obtained glass has abundant Si–OH groups on its surface that offers active sites for later functionalization [7,8]. Bioactive glasses are usually thermal-treated in order to stabilize its chemical structure forming a vitroceramic state [8].

Part of the initial evaluations that must be carried out on biomaterials is their ability to form an apatite layer on its surface, a study called bioactivity. This material behavior can be measured through bioactivity test reported by Kokubo et al. (2006) [11]. The test consists on submerging the material in SBF in different periods of time to allow an apatite formation. Sol–gel derived bioactive vitroceramics can induce the formation of a bone-like apatite layer due to the presence of OH^- groups on their surfaces, which are able to produce hydroxyapatite nucleation [7,12].

An *in vitro* study by Oliveira et al. (2013) [13] presented that a bioactive vitroceramic in a ternary system SiO_2–CaO–P_2O_5 with molar fraction 60%–36%–4%, respectively, induces a fast formation of a hydroxycarbonate apatite layer in the presence of SBF, which means that this composition is a potential application for tissue engineering. In previous work, we reported that a bioactive vitroceramic in the same system 60% SiO_2–34% CaO–6% P_2O_5 (%mol.) presented an appropriate net formation without the presence of undesirable phases [14]. We also proved that it is possible to obtain bioactive vitroceramics using alternative precursors such as acetate precursors, as net modifiers given that conventional glasses are synthesized with calcium nitrate that form a non-homogeneous glass [15].

In this study, a vitroceramic in a ternary system was synthesized through sol–gel route using non-conventional calcium and phosphorous precursors according to our previous work [14]. In this vitroceramic was evaluated the bioactive behavior in SBF and the formed layer, identifying how similar is the layer with bone natural apatite in order to promote its use in bone tissue engineering.

Materials and Methods

Materials

Ammonium dihydrogen phosphate (ADP, $NH_4H_2PO_4$) was purchased from Carlo Erba Reagent. Tetraethylorthosilicate (TEOS, $C_8H_{20}O_4Si$) and calcium acetate (CaAc, $Ca(CH_3COO)_2$) were purchased from Merck Inc. and ethanol (C_2H_6O) from Panreac. All chemicals used to prepare the SBF were provided from Sigma-Aldrich, Germany.

Vitroceramic synthesis

Vitroceramic (VC) was synthesized according to our previous work [14] following the reported by Vaid and Murugavel (2013) [16]. First, TEOS was added into a mixture of ethanol/distilled water and stirred until complete homogenization. This lasted approximately 1 h. Subsequently, ADP was incorporated into the previous solution and dissolved for 45 min. Then, CaAc was included, followed by the slow addition of an acetic acid/distilled water solution. The mixture was left in stirring for 5 h to reach the gel point and then was kept in a PET container for 3 days at room temperature to promote reagents react completely.

Finally, the gel was heated at 120 °C for 2 days to remove all the water content and eventually it was manually macerated to obtain a dry powder. For further use and characterization, the VC was washed to eliminate organic components and thermal treated in two stages for VC stabilization: (i) 400 °C/60 min with a heating rate of 26.67 °C/min, (ii) 600 °C/540 min with a heating rate of 3.33 °C/min. Additionally, a different thermal treatment (1050 °C/720 min) was used in order to crystalize the structure obtaining more define peaks only for XRD analysis.

Vitroceramic characterization

The synthesized VC was analyzed by X-ray diffraction (XRD) with XPert PANalytical Empyrean Series II diffractometer with voltage and current settings of 45 kV and 40 mA, respectively, and used Cu-Kα radiation (1.5405980 Å). Data were collected from 2θ= 5° to 60°. The phases were identified by comparing with previously reported sol–gel derived bioactive vitroceramics.

Fourier Transform Infrared (FTIR) also was recorded for the obtained vitroceramic powders using transmission mode in a Shimadzu IRTracer-100 by the method of attenuated total reflection (ATR) in the range 4000–400 cm^{-1}.

For the collection of Raman spectra a confocal Raman microscope (LabRam, Horiba, Jobin-Yvon, France) consisting a point focus 633 nm He–Ne laser source, which had an output power of 17 mW at the sample. Photons scattered by the sample were dispersed by 600 lines/mm grating monochromator, and simultaneously collected on a CCD camera with resolution of 1024 × 256 pixels, the spectra collection setup was 50 s in three different places to evaluate homogeneity of the synthesized powder.

The morphology and microstructure of the VC was analyzed by SEM. The samples were coated with a thin layer of Gold (Au) by sputtering (DENTON VACUUM Desk IV) and then they were observed on a Scanning Electron Microscopy (JOEL-JSM 6490 LV) that operated at an acceleration voltage of 20 kV. This microscope is associated to an energy dispersive EDX (INCA PentaFETx3 Oxford Instruments) spectrometer equipment. The measures were performed following the same conditions to each sample, using the same acceleration voltage and selecting similar places in morphology in order to obtain comparable results.

Finally, VC density was measured conforming to ASTM D2320-98 with distilled water as wetting agent.

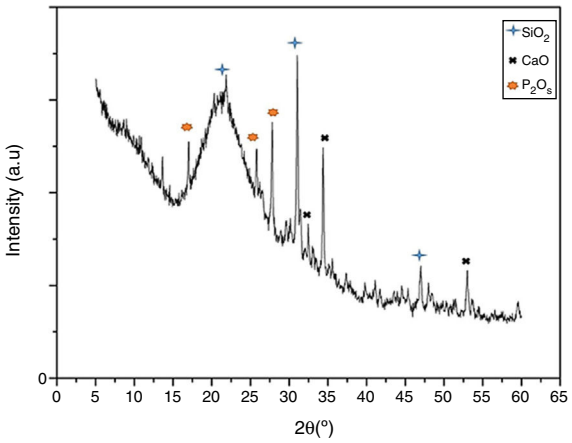

Figure 1 – XRD result of synthesized VC.

In vitro bioactivity study

The obtained powder of VC mentioned in Vitroceramic synthesis section was uniaxially pressed at 30 MPa for 2 min in order to obtain cylindrical disks with a diameter of 10 mm and thickness of 2 mm. The cylinders were immersed in the SBF solution prepared according to Kokubo and Takadama (2006) [11] and incubated at 37 °C in closed and static tubes for 7 and 14 days. The volume of SBF used during the test was calculated according to the relation: SBF volume (mL) = 10% discs mass (mg) [17]. There were two disks for each day of study and they were placed in different tubes to ensure independence on the results. Afterwards, the cylinders were removed from the SBF solution and washed with distilled water to remove undissolved salts. The submerged discs were analyzed by XRD, FTIR, SEM and EDX with the same equipment mentioned above without previous treatment. ImageJ software was used to analyze SEM results by taking 10 images per sample to perform a covered area study.

Results and discussion

Vitroceramic characterization results

Fig. 1 presents the XRD spectrum for the synthesized VC after crystallization by heat-treatment at 1050 °C. The figure shows narrow and differentiable peaks comparable with previously reported peaks for similar systems (SiO_2–CaO–P_2O_5) [1,18]. Those peaks are centered at approximately 30.9 and 21.3 (2θ) for primary and secondary peaks of SiO_2, respectively, forming a cristobalite phase. Those at 34.4 and 31.3 are primary and secondary for CaO, and those at 27.7 and 25.7 are for P_2O_5. Moreover, it can be seen that no undesirable peaks associated to pseudo-wollastonite pattern are formed [19] which could appear because of the chemical nature of oxides involved in vitroceramics synthesis. This result indicates the formation of a pure vitroceramic phase.

FTIR was performed in order to identify the main functional groups of the VC. Fig. 2 shows the obtained FTIR spectrum where a strong band between 1400 and 840 cm^{-1} centered at

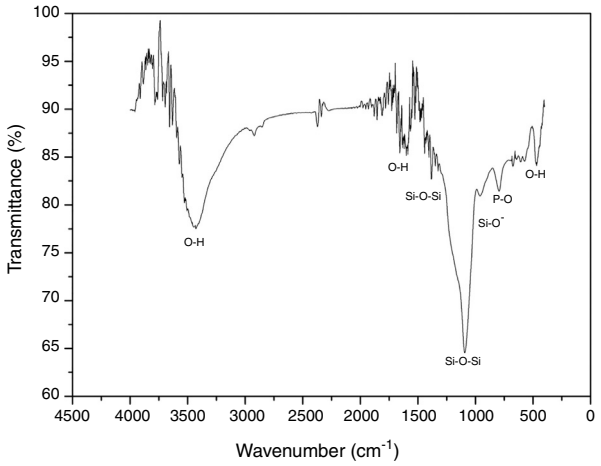

Figure 2 – FTIR spectrum of synthesized VC.

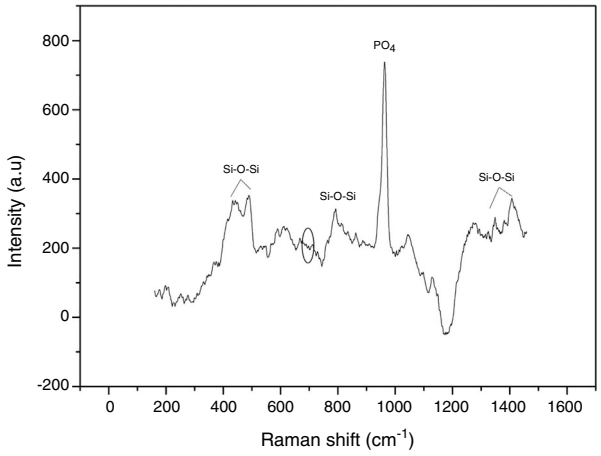

Figure 3 – Raman spectrum of synthesized VC after 600 °C heat treatment.

around 1097 cm^{-1} can be related to the formation of a silicon net. According to the literature, 1396 and 1097 cm^{-1} bands are attributed to asymmetric stretching of Si–O–Si group; whereas the band at 953 cm^{-1} corresponds to the Si–O^{-} vibration [20]. In addition, band at 792 cm^{-1} is associated to vibration mode of P–O bond and bands at 3450, 1600 and 470 cm^{-1} are the O–H vibrations [21]. Also, it can be seen that the synthesized VC presented no organic components on the spectrum due to final wash during synthesis process.

Raman spectroscopy was used to identify the formed vibrational groups of synthesized VC after stabilization by heat-treatment at 600 °C. Fig. 3 shows the obtained spectrum in one of the evaluated points, where the absence of the 643–654 cm^{-1} band evidenced the complete hydrolysis of TEOS precursor to silanol [20]. Additionally, the presence of 424 and 489 cm^{-1} bands are an indicator of silanol condensation into silane or siloxane with Si–O–Si bonds. Generally, bands between 800 and 1450 cm^{-1} are related to Si–O–Si bond in tetrahedral silicates. On the other hand, an intense band at 958 cm^{-1} is due to PO_4 group vibration and possibly masks another peak at 920 cm^{-1} belonging to silicon. This result indicates the correct vitroceramic synthesis, and also proves the VC homogeneity that gives the same spectra obtained in each analyzed point [20,22].

In Fig. 4, we report SEM micrographs of VC powder after stabilization heat-treatment at four different magnification scales. As is shown in the images, the synthesized VC, with a density of 1.80407 ± 0.01 g/cm^3 (25 °C) comparable with cortical bone apparent density (1.85 g/cm^3) [23,24], is highly agglomerated even in highest magnification, which does not allow to define particle size or morphology. In contrast, it can be seen that the whole sample remained in a homogeneous state during the test given that the same morphology was found in the different taken images.

Fig. 4c and d shows a complex morphology of synthetized VC because structures, such as rods, bars or whiskers, are not feasible to determine including its size measurement of each dimension. Comparing all the analyzed images, same structures and distributions can be seen proving morphological homogeneity on the sample. Nevertheless, its important result due to natural hydroxyapatite is nano-size with similar shape of rods [25], which means that synthesized VC could be used as bone replacement. Both SEM and Raman results proved chemical and morphological homogeneity of synthesized VC.

Bioactivity behavior results

In order to evaluate bioactivity the first step was to determine the formation of an apatite layer over VC disk surface. This assessment was performed with SEM images and EDX analysis. Fig. 5 shows the obtained images and EDX analysis for VC after 7 and 14 days in SBF solution, all the acquired images were analyzed with Image J software to quantify the covered surface. The images show an increase of the formed precipitates from 7 to 14 days, indicating that the amount of precipitates on VC surface rise from $9.655 \pm 0.5\%$ to $13.855 \pm 0.5\%$ of the coated surface.

The precipitates were analyzed through EDX in three different places with the same morphology and the same work voltage to assure homogeneous results. Calcium and phosphorous ratio (Ca/P) was calculated with the EDX results at 7 and 14 days. The obtained value at 14 days in SBF indicates a similarity between formed precipitates and natural hydroxyapatite that varies in the range 1.37–1.87 according to Wu et al. [26]. These results show that the synthesized VC allows the formation of precipitates on its surface and they increase with time exposition in SBF. In addition, Ca/P ratio indicates that the layer could be apatite precipitates, which means that VC is appropriate for bone tissue engineering.

In Fig. 6, there are SEM images of VC discs cross-section view before and after SBF treatment. A thin apatite deposit on 14 days disk can be seen which proves bioactive behavior of synthesized VC which is in accordance with the above mentioned fact about apatite formation on VC surface.

Fig. 7 shows the SEM image of the apatite formation after 14 days in SBF in order to analyze its morphology. It can be seen that agglomerates in different sizes are difficult to measure real size of the particle. However, it seems that the particle has a small size, approximately less than 2 μm, and that high agglomeration is desirable for bone tissue applications given that natural apatite presents micro and nanosizes [26,27] and

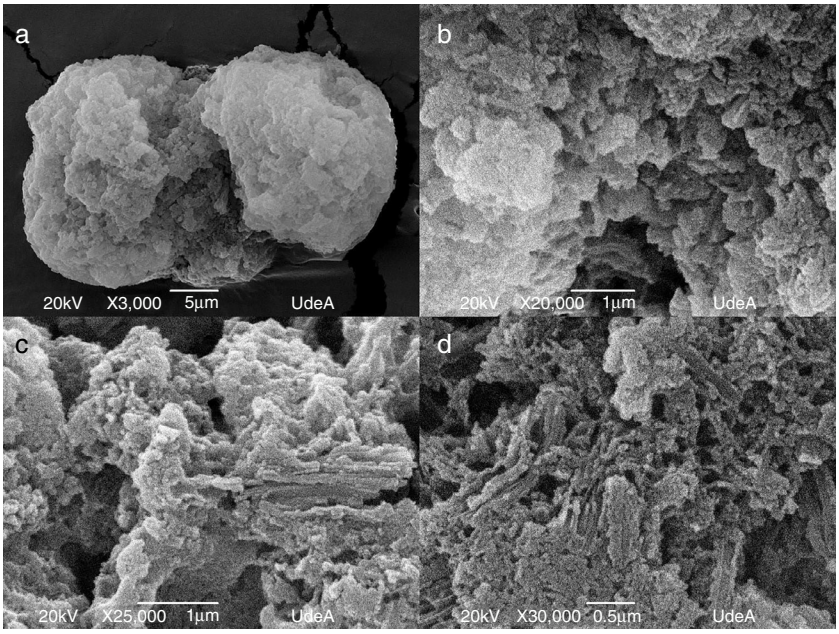

Figure 4 – SEM micrographs of synthesized VC at different magnifications of a) X3000, b) X20000, c) X25000 and d) X30000.

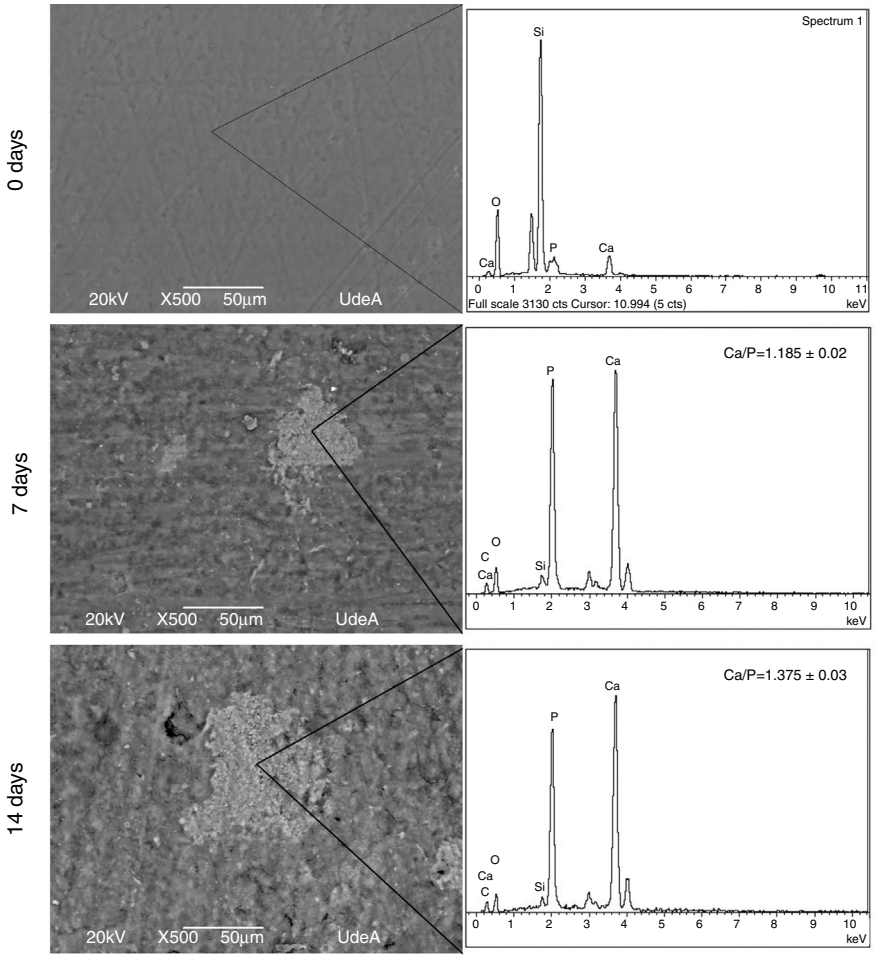

Figure 5 – SEM images and EDX spectra of VC at 0, 7 and 14 days in SBF solution.

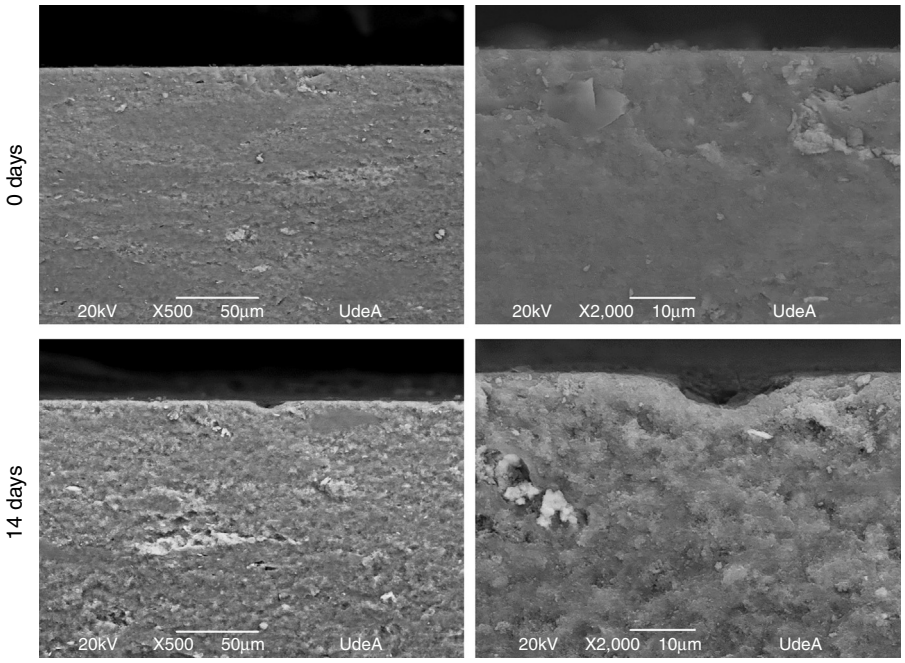

Figure 6 – SEM images of sectional view of VC disk at 0 and 14 days in SBF solution.

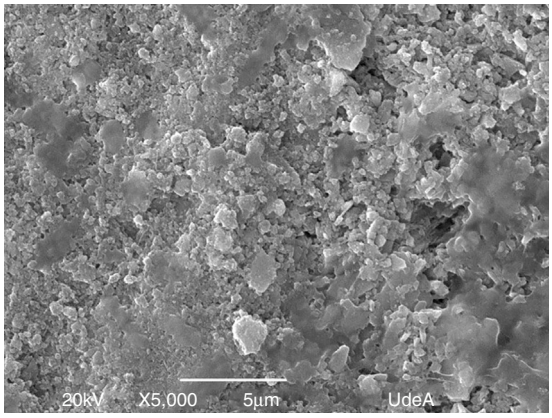

Figure 7 – SEM image of formed apatite layer on VC surface at 14 days in SBF.

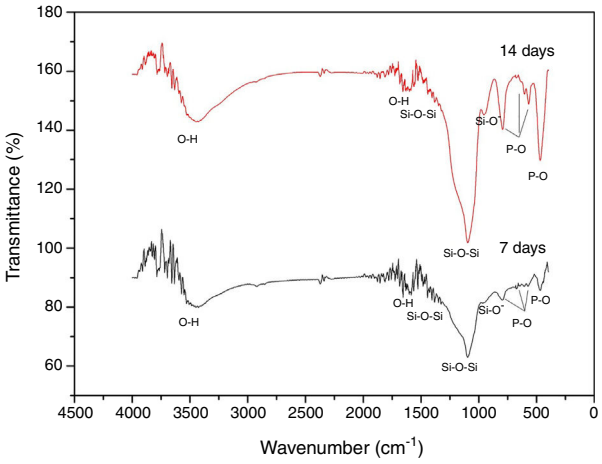

Figure 8 – FTIR analysis of formed layer on VC surface after 7 and 14 days in SBF.

different levels of aggregation according to the position and role of each type of bone [28]. FTIR and XRD analysis were performed on the apatite to identify functional groups and crystallinity, respectively.

Fig. 8 shows the FTIR spectra of the formed superficial deposit at 7 and 14 days in SBF. There are bands on the spectra related to silicon group vibrations as mentioned previously at 1396, 1097 and 947 cm^{-1} and two bands belonging to O–H vibration at 1600 and 3446 cm^{-1} on both spectra.

Additionally, at 7 and 14 days on SBF, there are three bands found at 465, 568 and 601 cm^{-1} related to P–O bond vibrations belonging to PO_4^{-3} groups. Furthermore, there is a band at 792 cm^{-1} due to P–O bond stretching, which indicates the presence of crystalline phases of calcium phosphate associated to an apatite deposit formation on VC surface [29]. These bands increase with time exposition in SBF, which is in agreement with SEM analysis about layer growth on the surface.

Fig. 9 shows XRD spectra obtained on VC at stabilization temperature (600 °C), after 7 and 14 days in SBF. This study was carried out to obtain information of the formed precipitates about its crystalline nature. These VCs require a previous stabilization heat treatment however it is not enough to completely crystalize the structure. In the case of VC at 0 days, lower crystallinity was observed with heat treatment at 600 °C confirming the above suggestion, but the representative peaks of this VC were evidenced at a higher thermal treatment (Fig. 1). After 7 days in SBF, it can be seen that there is a strong and defined peak at around 2θ=28° that is possible due to the formation of calcium phosphate ($Ca_2O_2P_7$) identify with COD

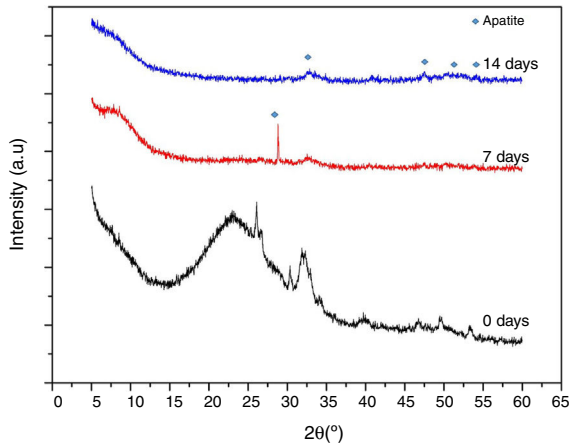

Figure 9 – XRD analysis of formed apatite precipitates on VC surface at 0, 7 and 14 days in SBF.

(crystallography open database) reference code 00-003-0604 in HighScore Plus software. However, this peak disappears at 14 days of exposition, since at this moment probably the formed deposit transforms into hydroxyapatite. The intense peak at 2θ=32° attributed to the (211) reflection in both 7 and 14 days in SBF proves the formation of such hydroxyapatite [30]. An increase of crystallinity is observed with time exposition in SBF, supported by the presence of additional peaks in the range 2θ=45–55°, which are characteristics of hydroxyapatite formation [31]. This result validates the appropriate behavior of synthesized VC for bone tissue engineering by forming hydroxyapatite in the presence of simulated fluid.

Conclusions

In this study, VC in a ternary system was synthesized by sol–gel route at room temperature according to a previous work using non-conventional precursors such as calcium acetate and ammonium dihydrogen phosphate in order to evaluate its bioactivity behavior in the presence of simulated body fluid.

The results showed that it is possible to obtain bioactive vitroceramic using non-standard precursors proved by the analysis made which demonstrated the correct formation of a net of bioactive vitroceramic. Such results evidence that both calcium acetate and ammonium dihydrogen phosphate are appropriate alternatives for bioactive vitroceramic synthesis.

The VC presented good *in vitro* response by allowing an apatite formation on its surface in the presence of simulated fluid. Furthermore, the formed deposit seemed to be a calcium-deficient hydroxyapatite with Ca/P ratio close to natural apatite and with an appropriate crystallinity for bone tissue applications.

Conflicts of interest

The authors declare no conflicts of interest.

Acknowledgment

The authors thank Biomaterials Research Group and Gimacyr Research Group who helped during the bioactive glass synthesis process.

REFERENCES

[1] M. Dziadek, B. Zagrajczuk, E. Menaszek, A. Wegrzynowicz, J. Pawlik, K. Cholewa-Kowalska, Gel-derived SiO2–CaO–P2O5 bioactive glasses and glass-ceramics modified by SrO addition, Ceram Int 42 (2016) 5842–5857, http://dx.doi.org/10.1016/j.ceramint.2015.12.128.

[2] C.D.F. Moreira, S.M. Carvalho, H.S. Mansur, M.M. Pereira, Thermogelling chitosan-collagen-bioactive glass nanoparticle hybrids as potential injectable systems for tissue engineering, Mater Sci Eng C 58 (2016) 1207–1216, http://dx.doi.org/10.1016/j.msec.2015.09.075.

[3] L.L. Hench, The story of bioglass, J Mater Sci Mater Med 17 (2006) 967–978, http://dx.doi.org/10.1007/s10856-006-0432-z.

[4] L.L. Hench, R.J. Splinter, W.C. Allen, T.K. Greenlee, Bonding mechanisms at the interface of ceramic prosthetic materials, J Biomed Mater Res 5 (1971) 117–141, http://dx.doi.org/10.1002/jbm.820050611.

[5] H.C. Li, D.G. Wang, J.H. Hu, C.Z. Chen, Influence of fluoride additions on biological and mechanical properties of Na_2O–CaO–SiO_2–P_2O_5 glass–ceramics, Mater Sci Eng C 35 (2014) 171–178, http://dx.doi.org/10.1016/j.msec.2013.10.028.

[6] J. Zhong, D.C. Greenspan, U. Corporation, Processing and properties of sol–gel bioactive glasses, Structure (2000) 694–701.

[7] M. Catauro, F. Bollino, R.A. Renella, F. Papale, Sol–gel synthesis of SiO_2–CaO–P_2O_5 glasses: influence of the heat treatment on their bioactivity and biocompatibility, Ceram Int 41 (2015) 12578–12588, http://dx.doi.org/10.1016/j.ceramint.2015.06.075.

[8] K. Zheng, A.R. Boccaccini, Sol–gel processing of bioactive glass nanoparticles: a review, Adv Colloid Interface Sci (2017) 1–11, http://dx.doi.org/10.1016/j.cis.2017.03.008.

[9] F. Baino, G. Novajra, V. Miguez-Pacheco, A.R. Boccaccini, C. Vitale-Brovarone, Bioactive glasses: special applications outside the skeletal system, J Non Cryst Solids 432 (2016) 15–30, http://dx.doi.org/10.1016/j.jnoncrysol.2015.02.015.

[10] W.-T. Lin, J.-C. Chen, Y.-C. Hsiao, C.-J. Shih, Re-crystallization of silica-based calcium phosphate glass prepared by sol–gel technique, Ceram Int 43 (2017) 13388–13393, http://dx.doi.org/10.1016/j.ceramint.2017.07.041.

[11] T. Kokubo, H. Takadama, How useful is SBF in predicting in vivo bone bioactivity? Biomaterials 27 (2006) 2907–2915, http://dx.doi.org/10.1016/j.biomaterials.2006.01.017.

[12] A. Balamurugan, G. Sockalingum, J. Michel, J. Faur??, V. Banchet, L. Wortham, et al., Synthesis and characterisation of sol gel derived bioactive glass for biomedical applications, Mater Lett 60 (2006) 3752–3757, http://dx.doi.org/10.1016/j.matlet.2006.03.102.

[13] A.A.R. de Oliveira, D.A. de Souza, L.L.S. Dias, S.M. de Carvalho, H.S. Mansur, M. de Magalhães Pereira, Synthesis, characterization and cytocompatibility of spherical bioactive glass nanoparticles for potential hard tissue engineering applications, Biomed Mater 8 (2013) 025011, http://dx.doi.org/10.1088/1748-6041/8/2/025011.

[14] L.A. Quintero, D.M. Escobar. Chemical composition effect of sol-gel derived bioactive glass over bioactivity behavior, in: M. Meyers, et al., eds. Proceedings of the 3rd Pan American Materials Congress. The Minerals, Metals & Materials Series.

Springer, Cham, 2017. pp. 11–19, https://doi.org/10.1007/978-3-319-52132-92.
[15] D. Fernando, N. Attik, M. Cresswell, I. Mokbel, N. Pradelle-Plasse, P. Jackson, et al., Influence of network modifiers in an acetate based sol–gel bioactive glass system, Microporous Mesoporous Mater 257 (2018) 99–109, http://dx.doi.org/10.1016/j.micromeso.2017.08.029.
[16] C. Vaid, S. Murugavel, Alkali oxide containing mesoporous bioactive glasses: synthesis, characterization and in vitro bioactivity, Mater Sci Eng C 33 (2013) 959–968, http://dx.doi.org/10.1016/j.msec.2012.11.028.
[17] J. Faure, R. Drevet, A. Lemelle, N. Ben Jaber, A. Tara, H. El Btaouri, et al., A new sol–gel synthesis of 45S5 bioactive glass using an organic acid as catalyst, Mater Sci Eng C 47 (2015) 407–412, http://dx.doi.org/10.1016/j.msec.2014.11.045.
[18] L. Desogus, A. Cuccu, S. Montinaro, R. Orrù, G. Cao, D. Bellucci, et al., Classical Bioglass® and innovative CaO-rich bioglass powders processed by spark plasma sintering: a comparative study, J Eur Ceram Soc 35 (2015) 4277–4285, http://dx.doi.org/10.1016/j.jeurceramsoc.2015.07.023.
[19] M. Catauro, A. Dell'Era, S. Vecchio Ciprioti, Synthesis, structural, spectroscopic and thermoanalytical study of sol–gel derived SiO_2–CaO–P_2O_5 gel and ceramic materials, Thermochim Acta 625 (2016) 20–27, http://dx.doi.org/10.1016/j.tca.2015.12.004.
[20] I. Atkinson, E.M. Anghel, L. Predoana, O.C. Mocioiu, L. Jecu, I. Raut, et al., Influence of ZnO addition on the structural, in vitro behavior and antimicrobial activity of sol–gel derived CaO–P_2O_5–SiO_2 bioactive glasses, Ceram Int 42 (2016) 3033–3045, http://dx.doi.org/10.1016/j.ceramint.2015.10.090.
[21] F. Naghizadeh, M.R. Abdul Kadir, A. Doostmohammadi, F. Roozbahani, N. Iqbal, M.M. Taheri, et al., Rice husk derived bioactive glass-ceramic as a functional bioceramic: synthesis, characterization and biological testing, J Non Cryst Solids 427 (2015) 54–61, http://dx.doi.org/10.1016/j.jnoncrysol.2015.07.017.
[22] D. Bellucci, G. Bolelli, V. Cannillo, A. Cattini, A. Sola, In situ Raman spectroscopy investigation of bioactive glass reactivity: simulated body fluid solution vs TRIS-buffered solution, Mater Charact 62 (2011) 1021–1028, http://dx.doi.org/10.1016/j.matchar.2011.07.008.
[23] Nist, Composition of Bone, Cortical (ICRP), (n.d.). http://www.physics.nist.gov/cgi-bin/Star/compos.pl?refer=ap&matno=120 (accessed May 15, 2017).
[24] P. Zioupos, R.B. Cook, J.R. Hutchinson, Some basic relationships between density values in cancellous and cortical bone, J Biomech 41 (2008) 1961–1968, http://dx.doi.org/10.1016/j.jbiomech.2008.03.025.
[25] M. Šupová, Substituted hydroxyapatites for biomedical applications: a review, Ceram Int 41 (2015) 9203–9231, http://dx.doi.org/10.1016/j.ceramint.2015.03.316.
[26] S. Wu, X. Liu, K.W.K. Yeung, C. Liu, X. Yang, Biomimetic porous scaffolds for bone tissue engineering, Mater Sci Eng Rep 80 (2014) 1–36, http://dx.doi.org/10.1016/j.mser.2014.04.001.
[27] W.M. Saltzman, Biomechanics, in: Biomedical Engineering: Bridging Medicine and Technology, Cambridge University Press, Cambridge, 2009, pp. 656.
[28] G. Pezzotti, A. Rondinella, E. Marin, W. Zhu, N.N. Aldini, G. Ulian, et al., Raman spectroscopic investigation on the molecular structure of apatite and collagen in osteoporotic cortical bone, J Mech Behav Biomed Mater 65 (2017) 264–273, http://dx.doi.org/10.1016/j.jmbbm.2016.08.030.
[29] G.M. Luz, L. Boesel, A. Del Campo, J.F. Mano, Micropatterning of bioactive glass nanoparticles on chitosan membranes for spatial controlled biomineralization, Langmuir 28 (2012) 6970–6977, http://dx.doi.org/10.1021/la300667g.
[30] K. Nazemi, P. Azadpour, F.a. Moztarzadeh, M. Urbanska, M. Mozafari, Tissue-engineered chitosan/bioactive glass bone scaffolds integrated with PLGA nanoparticles: a therapeutic design for on-demand drug delivery, Mater Lett 138 (2015) 16–20, http://dx.doi.org/10.1016/j.matlet.2014.09.086.
[31] M. Araújo, M. Miola, A. Venturello, G. Baldi, J. Pérez, E. Verné, Glass coatings on zirconia with enhanced bioactivity, J Eur Ceram Soc 36 (2016) 3201–3210, http://dx.doi.org/10.1016/j.jeurceramsoc.2016.04.042.